Numerical and analytic modelling of elastodynamic scattering within polycrystalline materials

A. Van Pamel, G. Sha, M. J. S. Lowe, et al.

Citation: The Journal of the Acoustical Society of America **143**, 2394 (2018); doi: 10.1121/1.5031008
View online: https://doi.org/10.1121/1.5031008
View Table of Contents: https://asa.scitation.org/toc/jas/143/4
Published by the Acoustical Society of America

Numerical and analytic modelling of elastodynamic scattering within polycrystalline materials

A. Van Pamel,[1,a)] G. Sha,[2] M. J. S. Lowe,[1] and S. I. Rokhlin[2]
[1]*Department of Mechanical Engineering, Imperial College London, Exhibition Road, London, SW7 2AZ, United Kingdom*
[2]*Department of Materials Science and Engineering, Edison Joining Technology Center, The Ohio State University, 1248 Arthur E. Adams Drive, Columbus, Ohio 43221, USA*

(Received 14 May 2017; revised 24 February 2018; accepted 11 March 2018; published online 25 April 2018)

The elastodynamic behavior of polycrystalline cubic materials is studied through the fundamental propagation properties, the attenuation and wave speed, of a longitudinal wave. Predictions made by different analytical models are compared to both numerical and experimental results. The numerical model is based on a three-dimensional Finite Element (FE) simulation which provides a full-physics solution to the scattering problem. The three main analytical models include the Far-Field Approximation (FFA), the Self-Consistent Approximation (SCA) to the reference medium, and the herein derived Second Order Approximation (SOA). The classic Stanke and Kino model is also included, which by comparison to the SOA, reveals the importance of the distribution of length-scales described in terms of the two-point correlation function in determining scattering behavior. Further comparison with the FE model demonstrates that the FFA provides a simple but satisfactory approximation, whereas the SOA shows all-around excellent agreement. The experimental wave velocity data evaluated against the SOA and SCA reveal a better agreement when the Voigt reference is used in second order models. The use of full-physics numerical simulations has enabled the study of wave behavior in these random media which will be important to inform the ongoing development of analytical models and the understanding of observations.
 https://doi.org/10.1121/1.5031008

[DDE] Pages: 2394–2408

I. INTRODUCTION

Almost all naturally occurring materials exhibit heterogeneity on some length scale, but a wave propagating within such a medium only becomes appreciably perturbed once the wavelength is comparable to its characteristic dimension.[1–4] When this occurs, waves no longer propagate freely but rather become scattered. Practical encounters of scattering are found at both macro scales by seismic waves and at micro scales by ultrasonic waves within biological tissue or metallic and ceramic materials. These latter materials exhibit a polycrystalline microstructure with spatially varying elastic properties due to contrasting crystallographic orientations between neighboring grains. In recent years, the aerospace and power generation industries have driven research to better understand scattering within metallic materials and improve both ultrasonic flaw detection[5–7] and ultrasonic material characterisation.[8–10]

Different aspects of ultrasonic characterization of materials with realistic microstructures have been addressed, such as materials with macrotexture[8] and duplex microstructures for titanium[9–12] and steel[13] alloys, comparison of ultrasonic and electron backscatter diffraction methods,[14] effects of applied stresses,[15] and general macroscopic anisotropy[16] on ultrasonic scattering; also, multiscattering[17,18] and the mode-converted[19] ultrasonic backscatter method have been investigated.

Due to its fundamental importance and relevance to practical applications, understanding both the elastic[1–3] and elastodynamic[4–19] behavior within polycrystalline materials remains of longstanding interest. Early studies on the latter have been extensively reviewed by Papadakis[20] and reported in Refs. 21–24. Stanke and Kino[24] presented the unified second order approximation (SOA) model for scattering in a polycrystal, based on the theories of Keller[22] and Karal and Keller,[23] providing the dispersion equation for a perturbed wavenumber capturing the various scattering regimes including the Rayleigh, stochastic, and geometric. The underlying SOA[24] refers to the account of second order perturbations on the small parameter ε. Alternatively, Weaver[25] developed a scattering model taking roots in quantum field theory and electromagnetic wave scattering[26,27] and obtained an equivalent dispersion equation to that of Stanke and Kino,[24] however, as will be discussed later, within the spatial frequency domain instead of the physical domain. Nonetheless, research remains ongoing today in pursuit of more accurate and more general solutions, including those which can account for a wider range of heterogeneities such as elongated grains,[10,11] duplex materials,[9–14] and macrotextures.[8,16]

Existing theoretical models, however, are inherently approximate due to the effects of multiple scattering and randomness of the medium. They have an ever-present scope for uncertainty, as theoretical models are limited by approximations in the order of material perturbations and their account of multiple scattering, while experimental

a)Electronic mail: m.lowe@imperial.ac.uk

measurements fully contain such effects. Subsequently, validating the applicability of these analytical theories of scattering has historically been hindered by the difficulty of obtaining sufficiently reliable experimental data where a factor of two in agreement is typically considered to be satisfactory.[4,5] Two main reasons for these experimental difficulties can be identified: the difficulty of accurately measuring coherent waves; the difficulty of accurately quantifying the statistical properties of the random materials.

Alternatively, progress in elastodynamic modelling of heterogeneous media using Finite Element (FE) methods[28–31] has recently enabled accurate studies of wave scattering within realistic volumes of polycrystalline materials. Such methods, in direct contrast to the aforementioned limitations, incorporate full-physics models, thereby including multiple scattering and enable ideal experiments with full control and knowledge of the random properties of the materials.

An opportunity thus exists to employ numerical methods to complement our understanding based on analytical findings and answer some of the remaining questions surrounding scattering approximations. This article employs recently developed full-physics three-dimensional (3D) numerical modeling and implements both classical and the latest analytical scattering models to evaluate various scattering approximations. The analytical scattering models are modified to include the generalized two-point correlation function determined from the simulated material systems used in the 3D numerical modeling. This evaluation serves to select the most appropriate models but in addition aims to provide useful insights into scattering behavior; this is fundamentally important to a variety of fields but is also practically relevant where encounters of scattering occur, such as seismics, acoustics, and non-destructive evaluation (NDE). In particular, an independent validation of the analytical models is relevant to inversion techniques which aim to infer microstructural properties from physical measurements.

Section II describes the analytical theories considered, before outlining the numerical methodology in Sec. III. The results in Sec. IV are structured in three parts: first, the numerical and analytical results convey the significance, beyond a mean characteristic, of the statistical distribution describing the heterogeneity in determining scattering behavior. Second, we evaluate the far field approximation (FFA) in its ability to provide a simpler implementation to the scattering problem. Finally, we compare the analytical and numerical model with experimental data to investigate the suitability of two varying effective reference medium approaches: the Voigt average or the self-consistent approach (SCA). This is followed by concluding remarks in Sec. V.

II. THEORY

Wave propagation and scattering in the established theoretical framework is described in terms of scattering induced attenuation α_L and dispersive phase velocity V_L, pertaining mathematically to the complex perturbed wavenumber for an infinite plane wave. Our current model description is general and suitable for arbitrary single-phase anisotropy of grains; however, the later comparison with the numerical model is given for the specific subset of equiaxed cubic grains.

A. Background: The dispersion equation in the spatial frequency domain

Following Stanke and Kino,[24] we call the model that we employ and further develop in this work the SOA. In Ref. 24, the dispersion equation is obtained in the physical domain and computations are performed for the exponential two-point correlation function $\exp(-r/a)$ where a is the correlation radius which is interpreted as the averaged radius of the equiaxed grains. Here we evaluate the dispersion equation in the spectral domain as was presented by Weaver.[25] However, Weaver did not consider solutions for the dispersion equations and instead employed the Born approximation whilst also considering the exponential correlation function. Solving the dispersion equation in the spectral domain involves computation of the Cauchy integrals, which complicates its evaluation. The values of the complex perturbed wavenumber were computed by the spectral method described by Calvet and Margerin[32] without solving the dispersion equation and instead computing maxima of the spectral function, however, also utilizing the aforementioned exponential correlation function.

In this work, we obtain and numerically solve the dispersion equation in the spectral domain but instead implement a general two-point correlation, which later enables an analytical fit to that to be obtained numerically from the FE models (discussed in Sec. III). To be sure that this works correctly in the implementation in this analytical model, we have made a direct comparison of its solution with that of the Stanke and Kino dispersion equation[24] for its specific case of an exponential correlation function $\exp(-r/a)$; the results are identical.

We compare the SOA model with the FE computations in a wide range of non-dimensional frequency of scattering regimes for the correlation function of numerically synthesized 3D polycrystals. In addition, we implement such "exact" correlation functions in two recently published models: the far field approximation (FFA) model[33] and the SCA,[34] and compare the three models, SOA, FFA, and SCA, under the same conditions with the FE results.

In our numerical and analytical models, we consider a completely dense aggregate of a random assembly of perfectly bonded crystallites (anisotropic grains) forming a polycrystalline medium in a 3D domain. The propagating wave scatters on grain boundaries due to misorientation of the crystallographic orientations of neighboring grains; this resulting in the loss of scattered energy from the propagating wave and leading to attenuation of the propagating wave. In the numerical model, for a given random model realization of the grain assembly, the scattering problem is solved numerically with a complete account of the grain geometry and boundary conditions between grains, and of multiple scattering effects, thus determining the wave velocity and attenuation. By computing wave propagation for numerous random realizations of grain orientations in the material model and averaging,[31] we obtain dependences of the

velocity and attenuation on frequency and grain size that are used to evaluate approximate analytical models; this is the objective of the present study.

Analytically, one can describe this complex stochastic scattering problem only with use of different model approximations (for an excellent review and background we refer to Refs. 24, 26, and 27). In the extension of the latest analytical models considered here, the micro-inhomogeneous elastic medium (polycrystal) is replaced by a continuous random medium described by a local elastic stiffness tensor $c_{ijkl}(\mathbf{X})$, which is a random function of spatial coordinates $\mathbf{X}(X,Y,Z)$. The medium is assumed to be statistically homogeneous and its local elastic stiffness tensor $c_{ijkl}(\mathbf{X})$ is represented as

$$c_{ijkl}(\mathbf{X}) = C_{ijkl} + \delta c_{ijkl}(\mathbf{X}), \tag{1}$$

$\delta c_{ijkl}(\mathbf{X})$ are small random fluctuations with zero mean,

$$\langle \delta c_{ijkl}(\mathbf{X}) \rangle = 0, \tag{2}$$

and $C_{ijkl} = \langle c_{ijkl}(\mathbf{X}) \rangle$ is the mean macroscopic elastic tensor. The bracket notation $\langle \cdot \rangle$ indicates spatial average. The mean elastic medium with tensor C_{ijkl} is called the reference medium.[25] While the mean tensor of the reference medium coincides with the Voigt average,[3] we do not assume that the reference medium corresponds to the homogenized polycrystal with physically correct static properties. In fact, as we will discuss later, the model itself provides an elastic static limit with modulus (velocity) below the Voigt[3] average and between the Hashin-Shtrikman[2] bounds (see also Ref. 24).

The time-harmonic wave propagation and scattering is described by a system of partial differential equations with random coefficients, which is not solvable even in the scalar case (for discussion of the problem see Refs. 22, 26, and 27). For this reason, instead of seeking a solution for Green's dyadic $G_{k\alpha}(\mathbf{X},\mathbf{X}';\omega)$, one considers a solution for the mean Green function $\langle G_{k\alpha}(\mathbf{X},\mathbf{X}') \rangle$ (the Green's function defines the displacement response at location $\mathbf{X}$ in the kth direction to a unit point load at point $\mathbf{X}'$ in the α direction; $\omega = 2\pi f, f$ is the frequency). Analysis of the averaged field in some work is termed "smoothing"[25,27] since the averaged field is much smoother than the total field that includes fluctuations.[27] For the mean Green function $\langle G_{k\alpha}(\mathbf{X},\mathbf{X}') \rangle$, the stochastic wave propagation equations for random media reduce to the Dyson integral equation[25,34]

$$\langle G_{k\alpha}(\mathbf{X},\mathbf{X}') \rangle = G^0_{k\alpha}(\mathbf{X},\mathbf{X}') + \int\int G^0_{k\beta}(\mathbf{X},\mathbf{Y}) M_{\beta j} \langle G_{j\alpha}(\mathbf{Z},\mathbf{X}') \rangle d^3Y d^3Z, \tag{3}$$

where $M_{\beta j}$ is historically called a mass operator.[26,27] Whereas the Dyson integral equation generates all multiple scattering events, the Mass operator comprises scattering paths with a specific topology, which may be described in terms of irreducible Feynman diagrams. In Eq. (3), the dyadic Green function $G^0_{k\alpha}(\mathbf{X},\mathbf{X}')$ is for the macroscopically homogeneous reference elastic medium described by the tensor C_{ijkl}.[25,34]

While not explicitly shown, the polycrystal random inhomogeneous properties are quantitatively represented in Eq. (3) by the two-point correlation function (TPCF) $\langle \delta c_{ijkl}(\mathbf{X}) \delta c_{\alpha\beta\gamma\delta}(\mathbf{X}') \rangle$[25] for the elastic tensor fluctuations δc_{ijkl} from Eq. (1). It is proportional to the probability density of two crystallographic orientations of grains at points $\mathbf{X},\mathbf{X}'$. The correlation function depends on grain size and morphology and, by describing the neighboring grain orientations, determines grain scattering.[24] Due to the assumption of the statistical homogeneity and macroscopic isotropy of the polycrystalline medium, the covariance can be factorized into tensorial and spatial parts[24,25]

$$\langle \delta c_{ijkl}(\mathbf{X}) \delta c_{\alpha\beta\gamma\delta}(\mathbf{X}') \rangle = \langle \delta c_{ijkl} \delta c_{\alpha\beta\gamma\delta} \rangle \, w(\mathbf{X}-\mathbf{X}'), \tag{4}$$

where $w(\mathbf{X}-\mathbf{X}')$ is a geometrical two-point correlation function (or autocorrelation function) describing the probability that the two points $\mathbf{X},\mathbf{X}'$ are in the same grain; it depends only on the difference $\mathbf{r} = \mathbf{X}-\mathbf{X}'$ between two vectors $\mathbf{X},\mathbf{X}'$(the distance and the orientation angle). The factorization in Eq. (4) is equivalent to the assumption that the tensorial part is independent of spatial location.

Further analyses show that the Dyson equation, Eq. (3), has the form of a convolution integral[26] and is solved for the mean field Green function $\langle \mathbf{G}(\mathbf{k}) \rangle$ in the spatial Fourier domain space[25,35]

$$\langle \mathbf{G}(\mathbf{k}) \rangle = \left[\mathbf{G}^0(\mathbf{k})^{-1} - \mathbf{M}(\mathbf{k}) \right]^{-1}, \tag{5}$$

where $\mathbf{G}^0(\mathbf{k},\omega) = \sum_{M=1}^{3} \mathbf{u}^M \mathbf{u}^M / (\omega^2 - k^2 V_M^2) = \sum_{M=1}^{3} g_M^o \mathbf{u}^M \mathbf{u}^M$ is the spatial Fourier transform of the Green functions for the homogenized (reference) anisotropic medium; $\mathbf{k} = \mathbf{p}k$ is the wave vector, and $\mathbf{p}$ is the unit wave normal vector. The sum over M indicates summation of the three possible propagating modes with the Green functions g_M^o for each of the modes M with the mutually orthogonal unit polarization vectors $\mathbf{u}^M$.

In this work, we consider elastically isotropic homogenized macroscopic polycrystalline media (the elastic texture is absent at macro scale); the general models with texture were considered in Ref. 35 for hexagonal texture and in Ref. 36 for general texture where the full anisotropic Green's function was employed. Due to elastic macroscopic isotropy, we consider macroscopic velocities as independent of the propagation angle. However, it is convenient to introduce an infinitely small macroscopic anisotropy and to consider the Green's dyadic $\mathbf{G}^0(\mathbf{k})$ for the reference medium in the form for anisotropic media, where the isotropic medium is obtained in the limit of negligible anisotropy. This allows easy selection of the wave polarization vectors and, as in Eq. (5), to decompose the Green function into three propagating modes.[33,35,36]

Our objective is to find a complex wave number, perturbed by scattering, of the ensemble-averaged propagating wave. The real part determines the wave velocity and the imaginary part the scattering-induced attenuation. The perturbed complex wave number for wave propagation in a given random medium is the root of the dispersion equation which is obtained[26,27] from the denominator of the mean Green function $\langle \mathbf{G}(\mathbf{k}) \rangle$, Eq. (5) (the existence of an additional root

associated with a highly attenuated wave was discussed in Ref. 26 and for elastic waves in Refs. 32 and 33). The Dyson equation, Eq. (3), and its solution, Eq. (5), are exact; however, the spatial Fourier transform of the mass operator $\mathbf{M}(\mathbf{k})$, representing multiple scattering, is given by a series that cannot be summed[26,27] in general. To obtain a tractable solution one needs to make some approximations of the mass operator.

Different approximation methods by Keller[22] (perturbation method), Bourret[26,37] (the diagrammatic method) and the first order smoothing approximation[27] of the mass operator essentially lead to the same results. Keller[22] has shown under which conditions his method is identical to that of Bourret (those special conditions were used in Ref. 24). The equivalency of those different methods was also discussed by Frisch.[27] Physical interpretation of the diagrammatic method[26,27,37] shows that those approximations result in summation of the one convergent multi-scattering infinite subsequence (from the infinite sequence of all scattering event diagrams) that accounts for double scattering inside each heterogeneity without recurrent visits. This approximation is valid for small elastic perturbations and propagation distances such that the incident wave is mostly coherent.[25–27] In this approximation, the dispersion equation for the propagating wave M with the perturbed wave number $\mathbf{k} = \mathbf{p}k$ and polarization vector $\mathbf{u}^M$ can be presented[33] in the form

$$k^2 = k_M^2 - \frac{1}{V_M^2} m_M(\mathbf{k}), \tag{6}$$

where

$$m_M(\mathbf{k}) = \frac{1}{\rho^2} u_\beta^M u_q^M k_\alpha k_l \sum_{N=1}^{3} \int g_N^0\left(\mathbf{k}^{S,N}\right) v_\gamma^{S,N} v_j^{S,N} k_\delta^{S,N} k_i^{S,N} \times \langle \delta c_{ijql} \delta c_{\alpha\beta\gamma\delta} \rangle W\left(\mathbf{k} - \mathbf{k}^{S,N}\right) d^3 k^{S,N}. \tag{7}$$

Its solution provides the complex wave number $k = \mathrm{Re}k + i\alpha$ of the perturbed propagating wave, where α is the attenuation coefficient, $\mathbf{p}$ the unit wave vector of the propagating wave, and V_M is the velocity in the reference medium; k_α, k_l are the wave vector components. The term $m_M(\mathbf{k})$ in Eq. (6) relates to the decomposition of the mass operator into three propagating modes.[32,35,36] It produces a perturbation term in the dispersion equation that results in perturbation of the wave number k relative to the propagation in the unperturbed reference medium with the wave number k_M. Due to elastic modulus fluctuation, the main propagating wave M scatters into three scattered waves $N = 1, 2, 3$, indicated by the superscript index S and summation over N in Eq. (7) (one of the scattered waves is the same type as M). Each of the scattered waves propagates with wave number $\mathbf{k}^{S,N} = k^{S,N}\mathbf{s}$ and its own polarization $\mathbf{v}^{S,N}$ vectors ($\mathbf{s}$ is a unit scattering wave vector). $W(\mathbf{k} - \mathbf{k}^{S,N})$ is the spatial Fourier transform of the geometrical two-point correlation function $w(\mathbf{X} - \mathbf{X}')$ in Eq. (4) and can be interpreted as the material spectral function which filters the spectral response of the main propagating wave.

Equations (6) and (7) are applicable to polycrystals with texture (anisotropic reference media) and nonequiaxed arbitrary anisotropic grains. Eventually, we will use the polycrystal with equiaxed grains and macroscopic isotropy with propagating pure longitudinal L and scattered longitudinal and transverse waves; the two scattered transverse waves have orthogonal polarizations and the same velocity.

B. Generalized representation of two-point correlation function

To compute the dispersion equation [Eqs. (6) and (7)], one should assume the form of the two-point correlation function $w(r)$ in Eq. (4) [spectral form $W(\mathbf{k} - \mathbf{k}^{S,N})$ in Eq. (7)]. *A priori*, it is not known for a given material system; however, it can be determined from an experiment.[1,11,36] The assumption of Poisson statistics[24,25] is usually used for modeling of wave propagation in random media, and under such assumption, the geometrical two-point correlation function $w(r)$ for the equiaxed scatters is obtained in the form $w(r) = \exp(-r/a)$.[24,25] The advantage of this assumption is in its simplicity because the correlation function depends only on one medium parameter, the correlation length a, which for polycrystals can be interpreted as the mean grain radius. On the other hand, the grains are deformed by the material forming in many practical cases, and these can be approximated by general ellipsoids; such cases are described by direction-dependent correlation functions.[9–12,14,38]

The application of ultrasonic models with stochastic media properties approximated by the exponential Poisson correlation function $w(r)$ has been shown to be successful to reasonably describe experimental ultrasonic backscattering and attenuation data for some material systems; however, the applicability of this approximation has been questioned by comparison with the experimental correlation functions.[38] Also, by comparing to experiments, it is unclear how each of the uncertainties contributes to the differences in the results, that is to say, whether it is the approximation of the model or the approximation of the medium that dominates. Thus, it is important for quantitative comparison of the analytical models with numerical simulations to approximate more accurately the actual two-point correlation functions of the simulated polycrystal used for the numerical calculations. We do so here by fitting an exponential series to the correlation function obtained directly from the simulated polycrystal. We will briefly outline the approach below; the description for the anisotropic two-point function approximation will be published in detail elsewhere. We represent the two-point correlation function as

$$w(r) = \sum_{i=1}^{n} A_i \exp\left(-\frac{r}{a_i}\right), \tag{8}$$

where A_i and a_i are constants.

Our objective is to fit the experimental two-point correlation function by the exponent series, Eq. (8), because of its simplicity for the analytical spectral representation $W(\mathbf{k} - \mathbf{k}^{S,N})$ in Eq. (7) and its utilization in the models. The sum of Eq. (8) should satisfy the following physical constraints:

$$\sum_{i=1}^{n} A_i = 1; \tag{9}$$

$$w'(r=\mathbf{0})=\sum_{i=1}^{n}\left(-\frac{A_i}{a_i}\right). \tag{10}$$

The first of these constraints follows from the correlation function definition and the second, as proven by Man *et al.*,[38] should be satisfied exactly for the general case. We do not attribute a physical meaning to each term of the representations in Eq. (8) (for example, positivity of the spectra or the requirement $|A_i|<1$) and we apply these general physical requirements only to the total sum of Eq. (8) of the two-point correlation function. Some insight into the meaning of the scale length a_i in Eq. (8) can be obtained considering the correlation function in Eq. (8) for an actual polycrystalline medium in the spatial spectral domain and comparing it to the corresponding spectrum for the Poisson correlation function that depends on a single length parameter. Each term of Eq. (8) essentially modifies the spatial spectrum of the corresponding polycrystal with the Poisson statistics, eventually representing the spectral characteristic of the actual polycrystalline medium with its correlation function fitted by the function in Eq. (8).

C. SOA: Dispersion equation for equiaxed grains with generalized correlation function

For computation, it is advantageous to present the mass operator [Eq. (7)] in the dispersion equation [Eq. (6)] in spherical coordinates.[33] Considering equiaxed grains, due to symmetry, the integrand will depend on one angle: the angle between the wave vectors of the incident (M) $\mathbf{k}$ and scattered $\mathbf{k}^{S,N}(N)$ waves. In this paper, we will consider a longitudinal propagating wave $M=L$. It scatters into a longitudinal and two transverse waves, the latter with equal velocities which can thus be combined into the one scattering transverse wave term; we indicate those scattering terms by sub-indices $L\to L, L\to T$ and the mass operator is represented as

$$m_L(k)=m_{L\to L}(k)+m_{L\to T}(k). \tag{11}$$

Substituting for the $W(\mathbf{k}-\mathbf{k}^{S,N})$, the generalized spectral representation of the two-point correlation function in Eq. (8), and using the notations of Refs. 33, 36, and 39, we obtain the longitudinal-to-longitudinal scattering term; the first term in Eq. (11),

$$\begin{aligned} m_{L\to L}(k)=\frac{k^2k_{0L}^3}{\rho^2V_{0L}^2}\Bigg\{&\frac{2}{\pi}P.V.\int_0^\infty\frac{\xi^4}{1-\xi^2}\\ &\times\int_{-1}^{+1}\Bigg[\sum_{j=1}^{N}A_ja_j^3\left\{\mathrm{Re}\left[f_{LL}\left(k,a_j,x,\xi\right)\right]\right.\\ &\left.+i\mathrm{Im}\left[f_{LL}\left(k,a_j,x,\xi\right)\right]\right\}\Bigg]dxd\xi\\ &+\int_{-1}^{+1}\Bigg[\sum_{j=1}^{N}A_ja_j^3\left\{\mathrm{Im}[f_{LL}(k,a_j,x,1)]\right.\\ &\left.-i\mathrm{Re}[f_{LL}(k,a_j,x,1)]\right\}\Bigg]dx\Bigg\}. \end{aligned} \tag{12}$$

Here, ξ is a non-dimensional integration variable, $x=\cos\theta$ and

$$\begin{aligned} f_{LL}\left(k,a_j,x,\xi\right)&=\frac{A_{LL}+B_{LL}x^2+C_{LL}x^4}{\left[\left(1+k^2a_j^2+\xi^2k_{0L}^2a_j^2\right)-2k\xi k_{0L}a_j^2x\right]^2};\\ f_{LL}(k,a_j,x,1)&=f_{LL}\left(k,a_j,x,\xi\right)|_{\xi=1}. \end{aligned}$$

The longitudinal-to-transverse wave scattering term of the mass operator $m_L(k)$ is

$$\begin{aligned} m_{L\to T}(k)=\frac{k^2k_{0T}^3}{\rho^2V_{0T}^2}\Bigg\{&\frac{2}{\pi}P.V.\int_0^\infty\frac{\xi^4}{1-\xi^2}\\ &\times\int_{-1}^{+1}\Bigg[\sum_{j=1}^{N}A_ja_j^3\left\{\mathrm{Re}\left[f_{LT}\left(k,a_j,x,\xi\right)\right]\right.\\ &\left.+i\mathrm{Im}\left[f_{LT}\left(k,a_j,x,\xi\right)\right]\right\}\Bigg]dxd\xi\\ &+\int_{-1}^{+1}\sum_{j=1}^{N}A_ja_j^3\left\{\mathrm{Im}[f_{LT}(k,a_j,x,1)]\right.\\ &\left.-i\mathrm{Re}[f_{LT}(k,a_j,x,1)]\right\}dx\Bigg\}, \end{aligned} \tag{13}$$

where

$$\begin{aligned} f_{LT}\left(k,a_j,x,\xi\right)&=\frac{A_{LT}+B_{LT}x^2+C_{LT}x^4}{\left[\left(1+k^2a_j^2+\xi^2k_{0T}^2a_j^2\right)-2k\xi k_{0T}a_j^2x\right]^2};\\ f_{LT}(k,a_j,x,1)&=f_{LT}\left(k,a_j,x,\xi\right)|_{\xi=1}. \end{aligned}$$

Those equations are for general anisotropy of equiaxed grains in polycrystalline material. Specific crystallographic symmetry and properties of grains are specified by coefficients $(A,B,C)_{LL,LT}$. For cubic crystallites, they are given by $A_{LL}=3c^2/175$, $B_{LL}=2c^2/175$, $A_{LT}=c^2/35$, $B_{LT}=2c^2/175$, $C_{LL}=-C_{LT}=c^2/525$, where $c=c_{11}-c_{12}-2c_{44}$ is the anisotropy factor.

Equations (11), (12), and (13) for the mass operator are substituted into the dispersion equation [Eq. (6)], which is solved for the perturbed complex wavenumber k of the propagating wave. For cubic polycrystals the numerical solution of the dispersion equation [Eq. (7)] with the mass operator representation [Eqs. (11)–(13)] for the perturbed wavenumber k is identical to that of the Stanke-Kino dispersion equation[24] when a single exponential correlation function $w(r)=\exp(-r/a)$ is assumed.

D. Far-field approximation (FFA): The mass operator and dispersion equation

The SOA model just described is relatively complex, especially for non-equiaxed grains. For this reason, we have also selected for comparison the FFA model,[33] which

includes further simplification of the mass operator and results in a much simpler dispersion equation suitable for all frequency ranges. Comparison[33] with the Stanke-Kino model[24] showed that it provides a reasonably accurate solution for the attenuation coefficient in all frequency ranges. In-depth review of this model is beyond the scope of this paper; we will only briefly outline further approximations of the mass operator and specify the dispersion equation for the perturbed complex wave number for the generalized representation of the two-point correlation function as described in Sec. II B.

First the inner products $IP_{M\to N}(\theta,\varphi) = \langle \delta c_{ijql}\delta c_{\alpha\beta\gamma\delta}\rangle \times u_\beta u_q p_\alpha p_l s_i s_\delta v_\gamma v_j$ in the mass operator [Eq. (7)] are factored approximately from the integrals.[33] Based on physical considerations, the pulled-out factor $Ip_{M\to M} = IP_{M\to M}(\mathbf{p})$ takes into account dominantly forward scattering at high frequency into the main propagating mode $N = M$ since in this frequency range scattering to the modes with $N \neq M$ is small. At low frequencies, the scattering of the propagating main longitudinal wave in all directions into transverse waves is dominant, so the angle-averaged inner products $Ip_{M\to N} = \langle IP_{M\to N}(\theta,\varphi)\rangle$ is taken. Next, the mass operator [Eq. (7)] is transformed from the spectral to the physical domain; this essentially leads to the FFA of the dispersion equation [Eq. (6) and (7)]

$$k^2(\mathbf{p}) = k_M^2 + k^2(\mathbf{p})\sum_{N=1}^{3}\frac{k_N^2 Q_{M\to N}}{\pi} \times \int \frac{\exp[ik_N r]}{r} w(\mathbf{r})\exp(-ik\mathbf{p}\cdot\mathbf{r})d^3\mathbf{r}, \tag{14}$$

where the normalized scattering elastic factors $Q_{M\to N}$ that determine scattering strength are introduced

$$Q_{M\to N} = Ip_{M\to N}/\left[4\rho^2 V_M^2 V_N^2\right]. \tag{15}$$

The elastic scattering factors $Q_{M\to N}$ determine scattering strength due to grain misorientation, which is controlled by grain anisotropy. The exponential term of the Fourier transform in Eq. (14) depends on the perturbed wave number $k(\mathbf{p})$. The $\exp[ik_N r]$ factor belongs to the Green function in the unperturbed reference medium, with the unperturbed wavenumber as the term belonging to the bare Green function. The perturbed wave number squared $k^2(\mathbf{p})$ equals the unperturbed wave number k_M^2 in the macroscopically homogenized (reference) medium, plus a perturbation term depending on the perturbation parameters $Q_{M\to N}$ and the perturbed wave number $k(\mathbf{p})$ and the propagation direction.

The dispersion Eq. (14) is for the general shape of the grains represented by the correlation function $w(\mathbf{r})$. It depends on the radius vector direction $\mathbf{r}$ that results in the dependence of the perturbed wave vector on the propagation direction $\mathbf{p}$. For the equiaxed grains, there is no dependence on the propagation direction, and for the generalized exponential series representation of the two-point correlation function [Eq. (8)], the integrals in Eq. (14) can be taken explicitly.[33] As a result, the dispersion equation for a longitudinal wave is reduced to a simple form

$$k^2 = k_L^2 + k_L^2\sum_{j=1}^{N} A_j\left(\frac{4Q_{L\to L}}{\frac{k^2}{k_L^2} - \left(1+\frac{i}{k_L a_j}\right)^2} + \frac{4Q_{L\to T}}{\frac{k^2}{k_T^2} - \left(1+\frac{i}{k_T a_j}\right)^2}\right), \tag{16}$$

where A_j and a_j are defined in Eq. (8) and for cubic crystallites $Q_{L\to L} = 4c^2/(525\rho^2 V_{0L}^4)$, $Q_{L\to T} = c^2/(125\rho^2 V_{0L}^2 V_{0T}^2)$. Equation (16) is suitable for all frequency ranges and for the exponential correlation function ($N = 1$) $w(r) = \exp(-r/a)$ that was compared to the Stanke-Kino model[24] in Ref. 33.

As was discussed in Ref. 33, the FFA mostly makes a difference to the near field adjacent to the scatterer, with little change to the scattered energy carried away from the scatterer. This results in a small effect on attenuation (the imaginary part of the perturbed wave number), as was supported by comparison with Ref. 24. However, the approximation shifts the low frequency limit of velocity to that of the Voigt velocity, thus shifting the whole dispersion curve (this shift can be corrected for).

E. Self-consistent reference medium

The basis of the Stanke-Kino[24] and Weaver[25] models is Eqs. (1) and (2), which introduce perturbed media with random fluctuations $\delta c_{ijkl}(\mathbf{X})$ around the mean $C_{ijkl} = \langle c_{ijkl}(\mathbf{X})\rangle$. The polycrystal is replaced by a continuous random medium with no physical grains and boundaries between them (thus no need to satisfy boundary conditions). Different interpretations can be given to the $C_{ijkl} = \langle c_{ijkl}(\mathbf{X})\rangle$ relation as the wave scattering is concerned. The C_{ijkl} can be viewed locally, interpreting it as the directional moduli average of the anisotropic grain. All grains have the same directional average, thus forming the unperturbed reference medium; however, when the wave propagates, it sees different grain orientations at particular points in space, and so it scatters, which is accounted for by the random perturbation $\delta c_{ijkl}(\mathbf{X})$. As has been noted already by Stanke-Kino,[24] the wave sees grain effects differently in the Rayleigh and stochastic frequency ranges.

However, the most common interpretation of $C_{ijkl} = \langle c_{ijkl}(\mathbf{X})\rangle$ is to consider it as the Voigt[3] average for a static polycrystalline medium (with which it coincides) and as the upper bound for the medium's properties. This upper bound is above that implied by the actual elastic moduli of the homogenized polycrystal, which is supported by low frequency dynamic measurements and other experiments. Thus, one may consider replacing the Voigt[3] average reference medium by the self-consistent (SC) static medium, which more accurately represents the static elastic moduli, thus correspondingly modifying Eq. (1) and considering $\delta c_{ijkl}(\mathbf{X})$ to be a fluctuation from this background medium. Kube and Turner[34] have suggested and systematically employed this principle in their model. It is reasonable to assume that, at least at low frequency, due to averaging effects on the wavelength, the elastic properties will be close to those of

properly homogenized polycrystalline media. For a recent relevant review of different homogenization methods, see Ref. 40.

In the Kube-Turner approach, a SC homogenized elastic medium is taken as the reference medium.[34] In that work, they re-derived the basic equations in the model and have demonstrated that the Stanke-Kino[24] dispersion equation can be used if one assumes a correspondingly modified anisotropic factor for the grains in the polycrystal.[34] They have directly computed the Stanke-Kino dispersion equation by the appropriate replacement of the grain anisotropy factor as explained below.

As a result of analysis[34] the new anisotropy factor is defined for grains of cubic symmetry as

$$\gamma = c - h(3c_{11} - 3c_{12} + 4c_{44}), \tag{17}$$

where c is the anisotropy factor for a cubic crystal and

$$h = \frac{\left(c_{11} + 2c_{12} + 6C_{44}^{SC}\right)\left(c_{11} - c_{12} - 2C_{44}^{SC}\right)}{3\left[8\left(C_{44}^{SC}\right)^2 + 9c_{11}C_{44}^{SC} + (c_{11} - c_{12})(c_{11} + 2c_{12})\right]}. \tag{18}$$

The shear elastic modulus C_{44}^{SC} for the SC medium is determined from a cubic polynomial[34]

$$8(C_{44}^{SC})^3 + (5c_{11} + 4c_{12})(C_{44}^{SC})^2 - c_{44}(7c_{11} - 4c_{12})C_{44}^{SC} - c_{44}(c_{11} - c_{12})(c_{11} + 2c_{12}) = 0. \tag{19}$$

The effective longitudinal elastic modulus[34] for the SC model is

$$C_{11}^{SC} = [c_{12} + h(c_{11} - c_{12})] + 2c_{44}(1 + 2h) + 3\gamma/5, \tag{20}$$

and the Voigt V_{0L}^{V} and SC V_{0L}^{SC} velocities are obtained as usual $V_{0L}^{V} = \sqrt{C_{11}^{V}/\rho}$, $V_{0L}^{SC} = \sqrt{C_{11}^{SC}/\rho}$.

In Ref. 34, the SC form of the Stanke and Kino model was obtained by replacing the Voigt-average anisotropic factor c^2 and velocities by the SC quantities, i.e., γ^2 and V_{0L}^{SC}, V_{0T}^{SC}.

The model predicts consistently lower scattering due to an effective decrease of the anisotropic factor γ of the crystallites.[34] Kube and Turner[34] compared the results with the experiment and against the Stanke-Kino model[24] and found that in some cases, the modified model better represents experimental measurements. However, the comparison of the results is strongly dependent on the statistics (two-point correlation function) of the material which are usually unknown or not well-known because for the latter case, they are usually determined on a small set of surface grains of the sample. On the other hand, the theoretical difference in attenuation between the models of about 70%[34] is, in most cases, within the combined experimental uncertainty of material statistics (see Ref. 41) and ultrasonic measurements. Consequently, it is not possible to be conclusive about this model's performance versus that of the Stanke-Kino model. The possibility of deploying independent numerical models, which account for the boundary conditions between grains and complete multi-scattering, then becomes attractive to investigate the validity of these approaches. Due to the importance of the selection of the reference medium, for fundamental reasons we have selected this and the SOA models for careful numerical comparison.

In this work, we have compared the SCA model with the SOA and numerical models, employing the SOA dispersion equation [Eq. (6) and Eqs. (11)–(13)] for the SCA computation, with the same replacement as discussed above, of the Voigt-average parameters with those of SCA, using generalized correlation functions, Eq. (8), for numerically synthesized polycrystals for all models. To check our algorithm, we have reproduced the original computations in Ref. 34 using the exponential correlation function $w(r) = \exp(-r/a)$.

F. Static limits of velocity

In addition to the elastodynamic properties, we make later reference to the elastic properties of polycrystalline materials as the static limits of velocity, and therefore include the equations as derived by the SOA and SCA model. In parallel to the Stanke and Kino approach, we apply the Born approximation to the dispersion equations of SOA and SCA to obtain an analytical equation for the complex wave number at Rayleigh limit. The real part of the complex wave number provides the static limit of phase velocity, as shown in Ref. 24 with the correction of a misprint.[33]

Static limit of phase velocity from SOA

$$V_l^V = \frac{V_{0L}^V}{1 + \frac{2c^2}{375\left(C_{11}^0\right)^2}\left(2 + 3\frac{C_{11}^V}{C_{44}^V}\right)}, \tag{21}$$

where Voigt velocity $V_{0L}^{V} = \sqrt{C_{11}^{V}/\rho}$. $C_{11}^{V} = 1/5(3c_{11} + 2c_{12} + 4c_{44})$ and $C_{44}^{V} = 1/5(c_{11} - c_{12} + 3c_{44})$ are Voigt moduli for polycrystals with cubic constituents. Equation (21) thus provides a simple estimate of the homogenized static elastic modulus $C_{11} = \rho V_{0L}^2$.

The static limit of phase velocity from the SCA is acquired by replacing the Voigt velocity and modulus by those in the SC media

$$V_l^{SC} = \frac{V_{0L}^{SC}}{1 + \frac{2\gamma^2}{375\left(C_{11}^{SC}\right)^2}\left(2 + 3\frac{C_{11}^{SC}}{C_{44}^{SC}}\right)}. \tag{22}$$

III. NUMERICAL METHOD AND REPRESENTATION OF POLYCRYSTALS

FE methods are being used increasingly for the elastodynamic simulation of polycrystalline materials,[28–31] and are now capable of delivering accurate performance in realistic sample volumes in three dimensions. The methodology undertaken in the present work is fully communicated by the

authors in Refs. 30 and 31 (also see dependencies[43–45]) and therefore only a brief summary is provided here.

The approach[30,31] involves propagating longitudinal plane waves within a relatively slender rectangular cuboid of polycrystals, where waves are transmitted on one end and received at the other. The lateral faces of the cuboid are constrained such that the longitudinal wave in the slender cuboid can be considered to be an approximation of a plane wave in an infinite volume. The intention of this approach with its focus on plane waves is to concentrate on the wave propagation behavior without the complications of spatially-varying profiles, edges, and diffractions that arise when modelling the finite beams of real transducers; if the plane wave can be represented properly now, the adaptation of these models to realistic finite fields is assured because that step has already been long established. Although the numerical model solves the wave propagation problem for both the spatially coherent (ballistic) wave and the spatially incoherent, scattered (coda) waves, for our present purpose we only require the former coherent contribution to evaluate the scattering induced attenuation α_L and dispersive wave velocity V_L. Both these characteristics are calculated across a range of scattering regimes, represented by a ka, which varies from 10^{-1} to 10^{1}. In addition, a $k=0$ "zero-frequency" wave velocity is obtained employing a quasi-static implementation of our otherwise dynamic FE model; this is detailed in Sec. II C.

To begin the procedure, independent realizations of 3D cellular volumes representative of random polycrystals are numerically generated by employing the Voronoi algorithm. Each resulting random Voronoi tessellation requires sufficiently high discretization to satisfy convergence criteria and suppress numerical errors[29,30] such as numerical attenuation, also known as mesh scattering. Through evidence from previous studies, to reduce these numerical errors to negligible levels,[29,30] eight-noded cube elements with a maximum node separation Δd, where $\Delta d < a/10$ and $\Delta d < \lambda/10$, are adopted in a structured mesh for incorporation into the spatial FE formulation. Boundary conditions are subsequently applied to accommodate a longitudinal plane wave comprising symmetry boundary conditions along the four (largest) exterior faces, also with their normal perpendicular to the propagation direction. An explicit central difference time marching scheme then incrementally solves the system of equations in terms of displacement, at a time step defined by the well-known Courant–Friedrichs–Lewy (CFL) condition.

An advantage of this particular numerical implementation is its ability to efficiently generate independent realizations of random but statistically equivalent media, thereby enabling ensemble averaging to further our statistical considerations. In order to achieve a new random and independent sample, it has been suggested in Ref. 31 to randomly reshuffle the grain orientations [formally known by the orientation distribution function (ODF)], rather than generating a new random tessellation which would require re-meshing a model—a computationally expensive step in this process. Although our numerical simulations solve both the quasi-coherent (forward propagating) and incoherent scattered wave field, the analytical solutions considered describe the mean field propagation behavior. By spatially averaging the FE results in post-processing from several independent realizations, we are able to enhance the contribution of the desired coherent wave and suppress its small incoherent counterpart.

For each individual model, the post-processing step involves the calculation of α_L and V_L from the output time-displacement response of the two (smallest) exterior surfaces, with their normal parallel to the propagation direction. One surface corresponds to the excitation surface and the other to the reception surface, thereby emulating an experimental pitch-catch setup. Upon the application of a selected time-window to isolate the coherent transmitted $T(t)$ and received $R(t)$ waves, fast Fourier transforms compute $T(\omega)$ and $R(\omega)$, the spectral amplitudes and phases, to enable a frequency dependent calculation of the attenuation and phase velocity, respectively.

Complete numerical details of the FE models used here can be found in Table I. The statistics of the random grain properties produced by the above methodology, as described by the two-point correlation function $w(r)$, are particularly important as mentioned in Sec. II; calculation of $w(r)$ is discussed in the Sec. III B. First, we discuss the material models.

A. Material models

The FE methodology allows for general symmetry crystallites. Here we consider cubically anisotropic materials which contain equiaxed grains, producing locally scattering media with macroscopically isotropic properties such that they remain untextured. For instance, we represent equiaxed polycrystalline copper using the material properties $c_{11}=169.6$ GPa, $c_{12}=122.4$ GPa, $c_{44}=74.0$ GPa, and a density of 8935 kg/m^3($V_0=6000$ ms^{-1}, $\nu=0.33$, A $=3.2$).

In addition, however, instead of naturally occurring materials, we model fictitious materials to enable an isolated parametric variation of the intensity of the elastic perturbations whilst preserving its average characteristics. An alternative method that utilizes materials of varying scattering strength without conserving all other parameters would ultimately introduce additional and undesirable complexities which also influence scattering behavior. The procedure to obtain the fictitious material properties comprises the calculation of the single crystal elastic stiffness constants (SCESC) for an equivalent Voigt[3] referenced medium (the equations can be found in Ref. 42) with varying a predefined and desired elastic anisotropy coefficient, A, where $A=2c_{44}/(c_{11}-c_{12})$. Three fictitious materials are generated, with an equivalent average longitudinal Voigt velocity, V_0, and an increasing cubic elastic anisotropy coefficient A

TABLE I. Numerical FE model details.

Model Label	N115200	N11520
Centre-frequencies	1–4 MHz	1–10 MHz
Dimensions (mm)	$12\times12\times100$	$12\times12\times10$
Grains	115 200	11 520
Grain size (μm)	500	500
Degrees of Freedom	345×10^6	278×10^6

TABLE II. Material properties for fictitious cubic materials of varying anisotropy, A, and a constant density, Voigt velocity, and Poisson ratio ($\rho = 8000\ \mathrm{kgm}^{-3}$, $V_0 = 6000\ \mathrm{ms}^{-1}$, $\nu = 0.33$).

Material label	A 1.5	A 1.8	A 2.4
c_{11} (GPa)	262.1	251.7	237.1
c_{12} (GPa)	136.5	141.7	149.0
c_{44} (GPa)	95.3	100.5	107.8
c (GPa)	−65	−91	−127.5

of 1.5, 1.8, and 2.4; full details are shown in Table II, where in addition the anisotropy factor[24] $c = c_{11} - c_{22} - 2c_{44}$ is given.

B. Calculation of the two-point correlation function

The function $w(r)$ is obtained by randomizing the locations of multiple pairs of points, r_1 and r_2, within a volume (our cuboid model) of cells (our grains), and determining whether both points of each pair lie within a single grain; the result is then expressed as a function of r where $r = |r_1 - r_2|$, the distance of separation. The probability of this occurring decreases as the distance r increases, which is quantified by $w(r)$.

Numerical implementation is relatively straightforward, namely, by exploiting the definition of the Voronoi tessellation, the above method is equivalent to computing whether the centroid of the Voronoi-cell nearest to point r_2 is equal to that of point r_1. Through repetition of this process, analogous to a Monte-Carlo approach, the probability can be calculated that a line of distance r exists within a single grain. In this case, 10^5 samples per data point of r were sufficient for convergence to below 1%, and r is incrementally varied (approximately 30 steps) to produce a discrete sampling of $w(r)$ as shown in Fig. 1. In view of the large number of sampling points, the uncertainty of these values is very small, less than the size of the symbols used to mark the points. A continuous analytical fit is subsequently obtained using the functional form of Eq. (8) and produces the coefficients listed in Table III. The two-point correlation function,

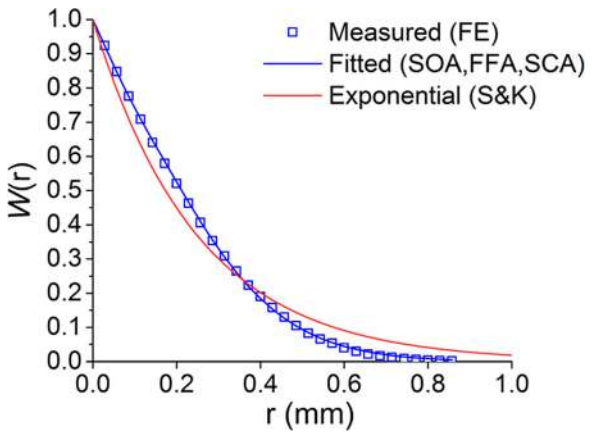

FIG. 1. (Color online) Two-point correlation function measured numerically for a 500 μm mean grain size FEM model including an analytical fit and a general exponential function. The models and their respective autocorrelation functions are indicated in brackets.

TABLE III. Coefficients of the two-point correlation function as shown in Eq. (8).

A_1	a_1	A_2	a_2	A_3	a_3	A_4	a_4
115.5	0.07548	−28.44	0.06455	157.1	0.09546	−243.2	0.08898

$w(r)$, is thereby obtained and shown in Fig. 1, enabling us to modify the theoretical scattering models outlined in Sec. II to match the statistical properties of the material in our numerical models. In addition, Fig. 1 shows an exponential two-point correlation function used in the Stanke and Kino (S&K) model (it depends on only one microstructure scale—the mean grain radius). The actual form of the two-point correlation function $w(r)$ depends on the method of numerical creation of the 3D polycrystal. In practice, it depends on the thermomechanical material processing during production and the microstructures obtained; as a result, the related two-point correlation function may be very different from that shown in Fig. 1. For example, Ref. 38 shows a case for rolled Al, when the exponential correlation function significantly overestimates the experimental values with a different trend than that shown in Fig. 1.

C. Quasi-static calculations

In addition to the dynamic simulations, a quasi-static analysis is performed to assess the pseudo-static wave velocity. Whereas static FE analysis is well established, the solution algorithms are quite different, and the solution of the static stiffness equations for these problems of vast numbers of degrees of freedom would be very costly in computer memory and processing. Furthermore, the FE programs that have been tuned for large computations have been developed quite differently for static and wave propagation applications, such that it would not be possible simply to make use of the same FE model just with different solution options. In our case, the particular FE program that was used for this study[44] has been tuned to achieve its efficiency just for explicit integration of dynamic behavior in the time domain. Thus an alternative approach was developed in order to use the dynamic implementation to achieve a quasi-static result.

In comparison to the previously outlined dynamic models, the spatial configuration for the quasi-static model remains much unchanged, only the external boundary conditions and forces are changed as illustrated in Fig. 2. The main alteration is the substitution of the previously applied tone-burst with a gradually applied static load F_s, such that our setup now resembles that of a uniaxial compression test. Whereas the symmetry boundary conditions remain unchanged on the four external surfaces, an additional symmetry condition is required and applied to what was previously the reception surface at the right-hand end of the domain in the figure, as shown in Fig. 2. Last, for the system to reach a static steady state, a damping coefficient is introduced into the material properties to gradually remove any dynamic contribution, which given sufficient time-steps, converges to a static displacement response, Δu_s, (or strain) to the applied force, F_s (or stress). The applied load and

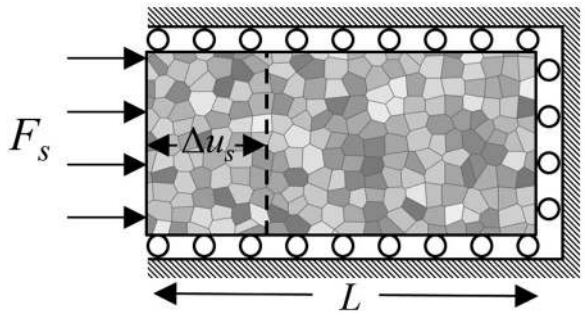

FIG. 2. Two-dimensional schematic of a 3D FEM uniaxial compression of a polycrystalline material under load, F_s, and a corresponding change in length, Δu_s. Not drawn to scale.

corresponding displacement can be reformulated into an applied stress and strain respectively, which enables us to calculate an effective Young's Modulus. Using the Newton-Laplace equation, $c = \sqrt{P/\rho}$, we can subsequently obtain a quasi-static wave velocity for compressional waves, V_s. Typical applied load $F(t)$ and its displacement response $U(t)$ is shown to convergence in Fig. 3. The methodology was tested first using a homogeneous material for which the static stiffness could be calculated perfectly by hand; this demonstrated performance to an equivalent degree of accuracy as achieved elsewhere in the modelling.

IV. RESULTS: EVALUATION OF SCATTERING APPROXIMATIONS

Sections IV A–IV C have the following purposes: (i) first we aim to demonstrate the influence of the two-point statistics describing the heterogeneities in determining scattering behavior; (ii) then we verify the FFA[33] and its value in offering a simplified and more accessible solution; (iii) and last we address the question of the most appropriate reference medium between a SCA[34] or Voigt[3] assumption.

We assess scattering behavior in terms of the attenuation, α_L, and dispersion of velocity, V_L, within cubic polycrystalline media using analytical, numerical, and

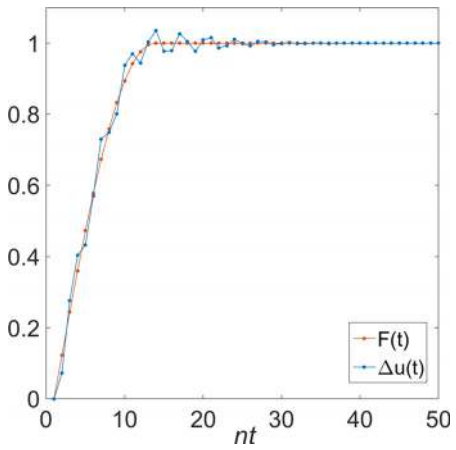

FIG. 3. (Color online) Typical input load, F, and quasi-static displacement response, Δu, at time step, nt, for a FEM uniaxial compression of a polycrystalline material. Both values are normalized against their respective convergence values, the static response represented by F_s and Δu_s in the calculation for the quasi-static wave speed.

experimental results for the coherent longitudinal wave. In particular, we consider three heterogeneous materials of gradually increasing elastic cubic anisotropy, A, comprising 1.5, 1.8, and 2.4, and in addition, polycrystalline copper. Table IV provides a summary of the analytical scattering models considered and detailed in Sec. II. The numerical methodology is outlined in Sec. III, and in each case, its results serve as an independent benchmark that represents the full-physics solution. The third set of results, experimental, makes use of velocity data from the literature.

A. Influence of the two-point correlation function

We demonstrate the influence of the two-point correlation function in determining scattering behavior as it remains a fundamentally and practically important question to our understanding of scattering. Scattering behavior as observed by the finite element model (FEM) is compared to a S&K[24] scattering model, which simply considers the mean grain size and assumes an exponential autocorrelation function, whereas the SOA conversely approximates the distribution of grain sizes using a fitted two-point correlation function that matches the statistical properties of the material in our numerical models.

Figure 4 plots the comparison of the normalized attenuation, αa_L, versus the normalized propagation constant, ka, where k denotes the wavenumber for fictitious polycrystalline materials; we use the familiar choice of normalization axes that have been used in the literature, such as in Ref. 24. Results are obtained for a wide range of ka such that the Rayleigh, transitional, and stochastic scattering behaviors are treated.

The first observation to note is that scattering increases according to the anisotropy coefficient for both models, as expected. Furthermore, a qualitative agreement is obtained by S&K theory, but this agreement can be seen to become much improved when considering a matching two-point correlation function as shown by the SOA. In addition to the average grain size, the two-point correlation function can thus be seen to play an important role in determining scattering behavior. This becomes most pronounced within the transitional and Rayleigh scattering regimes as can be seen from the change in slope, thus indicating a fundamental change in wavenumber or frequency dependence.

In the low-frequency Rayleigh limit, the S&K theory gives scattering dependence on the mean grain volume a^3,[24] whereas in the SOA model, the low frequency attenuation is proportional to $\sum_{i=1}^{N} A_i a_i^3$, thus showing dependence on the shape of the complete correlation function and enhancing the effect of larger microstructure scales a_i. As one can see

TABLE IV. Summary of the analytical models implemented (S&K, SCA, FFA) and developed (SOA).

Approximation:	S&K (Ref. 24)	SCA (Ref. 34)	FFA (Ref. 34)	SOA
Two-point correlation function	Exponential	Fitted	Fitted	Fitted
Reference medium	Voigt	Self-consistent	Voigt	Voigt
Scattering field	Full-field	Full-field	Far field only	Full-field

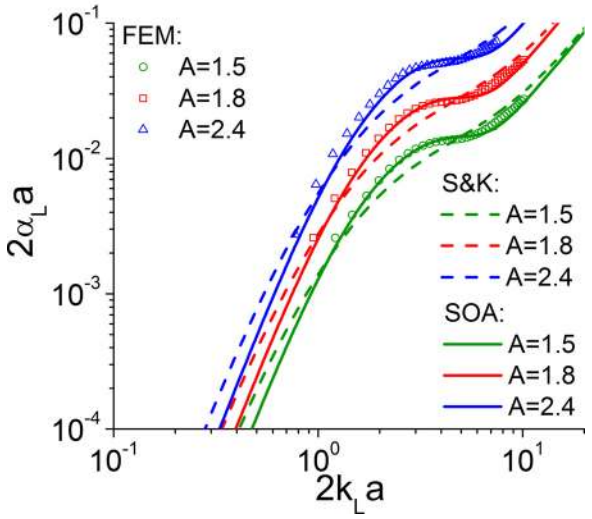

FIG. 4. (Color online) Normalized attenuation versus normalized propagation constant for fictitious polycrystalline materials of increasing anisotropy, comparing FEM, S&K, SOA.

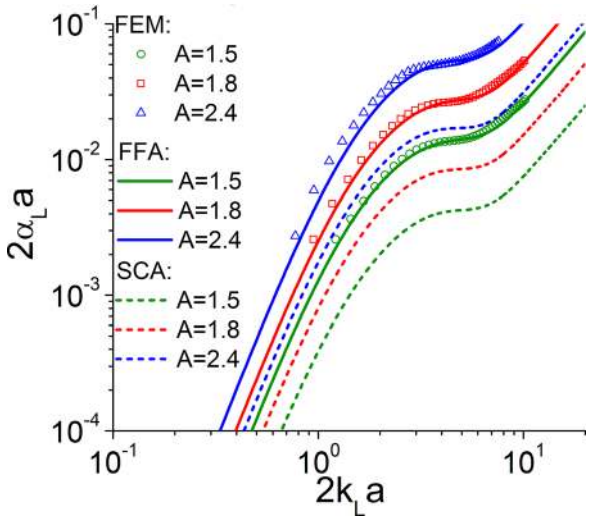

FIG. 6. (Color online) Normalized attenuation versus normalized propagation constant for fictitious polycrystalline materials of increasing anisotropy comparing FEM, SCA, and FFA.

in Fig. 1, the SOA model correlation function for a fixed $w(r)$ has lower corresponding r in the tail (large r) leading to smaller attenuation at lower frequencies compared to that in the S&K model (Fig. 4). In quantitative terms, the relative difference between SOA and FEM, hereon measured as $(Model - FEM)/FEM$, increases with anisotropy coefficient within the Rayleigh region from 6%, 22%, to 37%. This is expected and can be attributed to the increase of the material perturbation (wave scattering) and thus the effects of the approximation (albeit a superior one to the Stanke and Kino[24]) of the two-point correlation function (Fig. 1) and to the SOA approximation; and also to errors in the numerical discretization that worsen for the higher anisotropies due to the maximum wavenumber increasing. In the stochastic region, however, a better agreement is found which remains around 6% for all degrees of anisotropy.

Figure 5 plots the dispersive phase velocity, V_L, against the normalized wavenumber, ka, for the same fictitious materials treated in the previous figure. Both theoretical models now reveal a relatively small difference, rendering them practically inseparable for the purposes of our discussion. Nonetheless, the numerical results, both quasi-static and dynamic, show excellent matching with both theoretical models, where the better agreement is found for SOA in the present cases. The quasi-static result for each case is the leftmost data point on the plot, all other points are found from the dynamic simulations. At high ka values, the numerical results can be seen to deviate from their predicted behavior, which is probably due to numerical dispersion arising from discretization errors as the effective sampling rate decreases with increasing ka. Confirmation of this has not been pursued further because the difference is still small, and there is a huge computational burden in obtaining results for large ka, however, this will be investigated in future work.

The findings from both Figs. 4 and 5 are therefore in agreement. This provides further evidence in the validation of scattering theories such as the SOA, as found in a previous study.[31] However, more importantly here, it demonstrates the significance of a full description of the grain size statistics beyond the mean. This is particularly valuable

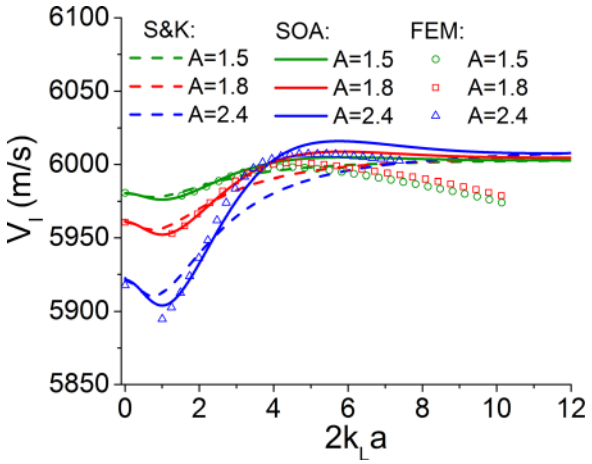

FIG. 5. (Color online) Phase velocity (ms^{-1}) versus normalized propagation constant for fictitious polycrystalline materials of increasing anisotropy, comparing FEM, S&K, SOA. Static-SOA results are included as per Eq. (21).

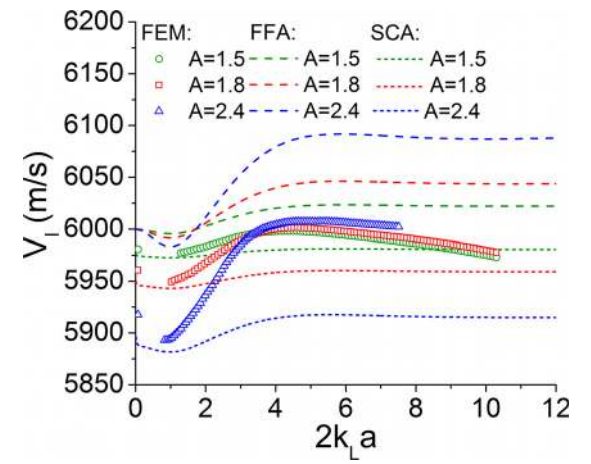

FIG. 7. (Color online) Phase velocity (ms^{-1}) versus normalized propagation constant for fictitious polycrystalline materials of increasing anisotropy comparing FEM, SCA, and FFA. Static-SCA results are included as per Eq. (22).

when considering applications for inversion from attenuation to material microstructure.

For the further studies to follow now, whether numerical or analytical, we evaluate scattering behavior on a uniquely equivalent basis, by modification of the assumed autocorrelation functions for the SOA, SCA, and FFA, to match the grain statistics generated by our numerical procedure.

B. Evaluation of the far-field approximation

The validity of the FFA[33] is assessed by comparison with the SOA model; the latter solves for the full scattering field, as does the FEM. As the SOA results have already been plotted in Sec. IV A, they are omitted for clarity from the proceeding Figs. 6 and 7 but will be included in the discussion.

Figures 6 and 7 plot the attenuation and phase velocity respectively for the fictitious materials treated previously. The FFA shows excellent agreement in terms of attenuation, the relative difference remains below 10% in all three scattering regimes when $A = 1.5$. At higher A, 1.8 and 2.4, the relative differences rises up to 37%. On a practical scale, these results are almost identical to the FEM and thus also, comparing with Figs. 4 and 5, to the SOA. In terms of phase velocity, Fig. 7 now reveals that the FFA consistently overestimates the result when compared to the FEM and thus also the SOA. However, this is to be expected because, as mentioned in Sec. II, neglecting near field effects shifts the solution of the dispersion equation towards the low-frequency velocity limit of the Voigt velocity, which is only an upper-bound limit, and therefore is not expected to deliver accurate results (the correction for this discrepancy is provided in Ref. 33).

C. Comparison of effective reference media

An important approximation which remains to be addressed concerns the theory for an effective reference medium. Such theories are useful to describe the average elastic[1–3] and elastodynamic[24,25,33,34] properties of a heterogeneous material. Here, we compare two second order scattering models, one employing a Voigt[3] referenced medium, the SOA; and alternatively the SCA,[34] both static solutions are given in Sec. II F. In addition to the previous fictitious materials, polycrystalline copper is considered by numerical, theoretical, and experimental means.

From the previously discussed Fig. 6, it can be seen that the SCA systematically underestimates the scattering for the cases tested here, typical errors are in the region 70%–80%, whilst the Voigt referenced medium, interpreted by the SOA, shows excellent agreement as mentioned earlier. In terms of phase velocity in Fig. 7, the SCA produces a closer agreement with the numerical FEM results (both quasi-static and dynamic) in comparison to the relative difference in Fig. 6; however, the SOA (Fig. 5) still outperforms the SCA on this occasion, thereby supporting the previous findings: the SOA, based on Voigt averaging, provides the most complete solution between the scattering theories considered here and for the cases studied here. The static results obtained from the SOA and SCA [Eqs. (21) and (22), respectively], shown as x in Figs. 4 and 7, add further confirmation that the SOA provides a satisfactory estimate in the zero-frequency limit for the elastic properties of polycrystalline materials.

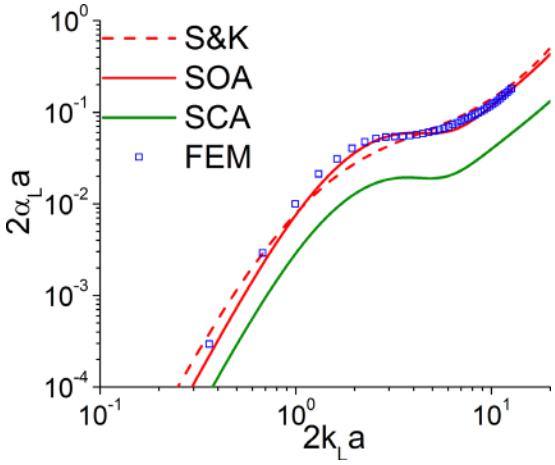

FIG. 8. (Color online) Normalized attenuation versus normalized propagation constant for polycrystalline copper comparing FEM, SOA, S&K, and SCA.

D. Agreement with experimental measurements of copper

In this final section, we bring another independent comparison, expand the range of cubic anisotropy considered, and add further evidence to determine the validity of the discussed approximations. We include results for a real polycrystalline material, copper, in addition to the aforementioned numerical and analytical models, making use of experimental results found in literature. Experimental measurements for wave velocity, performed by Ledbetter[46] for polycrystalline copper, are compared to the predictions of our previously mentioned models. Ledbetter's experimental results were chosen in particular as they represent the most

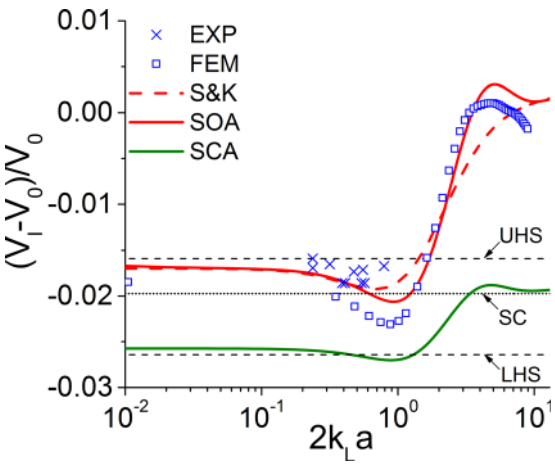

FIG. 9. (Color online) Voigt-normalized phase velocity versus normalized propagation constant for polycrystalline copper comparing numerical (FEM), theoretical (S&K, SOA, and SCA), and experimental measurements (EXP) from Ledbetter (Ref. 46). Three black lines indicate the quasi-static limits, two dashed "- - -" lines plot the UHS and LHS bounds, and the dotted "…" line shows the static SC averaging method. A single percentage (0.01) change on the y-axis corresponds to approximately 60 m/s.

complete and conclusive physical evidence available on the current matter and are believed to be of high accuracy. Whilst this and other experimental data had previously been available, a true comparison between the ability of different scattering theories to predict the measurements has not yet been possible, because of experimental errors and ambiguity in the two-point material statistics, now the deployment of the numerical modelling allows us to pursue such an evaluation.

Despite the absence of experimental results for attenuation, for completeness, we plot the attenuation results for copper using all the theoretical models in Fig. 8. Figure 9 plots the phase velocity for polycrystalline copper obtained by numerical, theoretical, and experimental[46] methods. In addition to the previously considered elastodynamic theories, we plot the quasi-static velocity limits as defined by the upper Hashin-Shtrickman (UHS) and lower Hashin-Shtrickman (LHS) second order bounds,[2] and the static SC result. The UHS and LHS provide a range for the theoretically possible wave velocities at low-frequency. It is therefore important that any predictions or measurements lie within this range. The static SC result, also plotted, provides a definite prediction for the quasi-static wave velocity.

In complement to the earlier findings of Sec. IV A, the results presented in Fig. 9 continue to agree with the previously observed trends; the contrast of SOA and S&K with the FEM predictions further reveals the beneficial impact of considering the appropriately representative grain size statistics, improving the confidence and extending the considered range of anisotropy to 3.2. The dynamic SCA solution continues to show a systematic offset. We can newly observe, however, an excellent agreement between the numerical FEM, theoretical SOA, and experimental measurements from Ledbetter;[46] the discrepancy remains below 0.6%. As a precautionary note, however, there is some uncertainty in the $2k_L a$ parameters for the experiment as no details are provided in Ref. 46 on the method of the given grain size measurement. The SOA model, as the second order model, performs its own low frequency homogenization of the medium that results in a low frequency velocity limit significantly below the Voigt velocity V_0 (V_0 corresponds to zero on the y-axis in Fig. 9). This low frequency SOA limit is between the Hashin-Shtrickman (HS) bounds and slightly above the quasi-static FEM and the static SC average, which show good agreement.

The dynamic SCA model also performs its own low frequency homogenization that results in a low frequency velocity limit well below the static SC average and the experimental and the quasi-static FEM results.

The discussion of the velocity limits in particular enables determining the suitability of the effective medium approximation. For this reason, we summarize the results from the fictitious and copper materials in Fig. 10, by replotting only the computed low-frequency velocity limits as a function of the anisotropy constant, A, for the various material systems considered. As can be seen, the FEM and SOA results remain within the theoretical HS bounds for all cases, whereas the SCA model produces a minor violation of the lower HS bound for the fictitious materials.

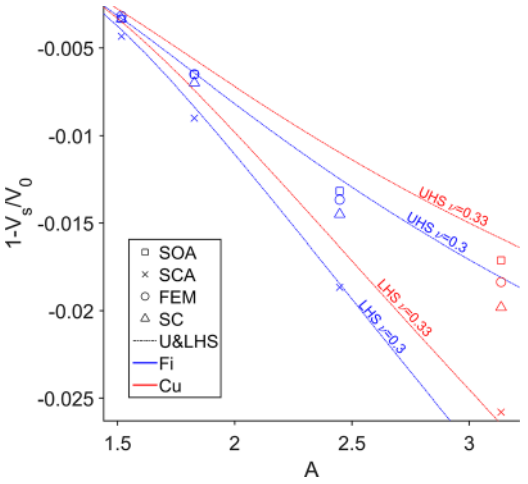

FIG. 10. (Color online) Voigt normalized low-frequency velocity limit versus cubic anisotropy, A, for the fictitious materials (Fi in blue/dark) and Copper (Cu in red/light) as predicted by the theoretical scattering models (SOA and SCA as square and x, respectively), numerical FEM model (as circle), and static SC averaging method (as triangle). The UHS and LHS bounds (as dashed) are plotted to convey the range of theoretically possible velocities for either material.

V. CONCLUSION

The elastodynamic scattering behavior of polycrystalline materials was studied across a wide spectrum of wavelengths including the Rayleigh, transitional, and stochastic regimes. Contributions from numerical, theoretical, and experimental evidence assessed the validity of the various scattering approximations found in literature and determined the influence of previously uninvestigated parameters on scattering behavior. The evolution of the scattering induced attenuation and dispersive phase velocity was obtained for cubic anisotropic polycrystals, represented by both fictitious and naturally occurring materials within a wide range of anisotropy factors of crystallites. In addition to providing a thorough background for the present state-of-the-art analytical scattering theories, this led to various findings. The study revealed the following:

- In addition to an average length-scale characteristic to represent the medium's heterogeneities, the distribution function of the length-scale plays an important role in determining scattering behavior. A quantitatively excellent agreement was reached when comparing numerical FEM and SOA theory for both scattering induced attenuation and phase velocity on a statistically equivalent basis. This result is particularly useful for future experimental approaches which aim to invert measurements to infer material properties.
- The FFA approximation offers a relatively simple analytical implementation of scattering for future studies, which was shown here to provide a good approximation to the attenuation characteristics although expected discrepancies were found in the prediction of phase velocity for the cases considered.
- Prior to this study, a certain ambiguity existed regarding the approximations to calculate the elastic properties for a valid reference medium (and thereby also its

perturbations). In this work, the Voigt reference medium was demonstrated to produce sufficiently accurate results for both attenuation and phase velocity, in comparison to an alternative SC reference medium approach which produced overly conservative estimates to scattering. These findings were supported by both numerical calculations undertaken in the paper and experimental measurements for velocity taken from literature.

In general, the levels of agreement between the numerical, experimental, and theoretical models were excellent and unprecedented. This adds further evidence to the existing literature by investigating a new range of material systems, that numerical approaches are now sufficiently mature to solve the 3D elastodynamic scattering problem. The authors believe these findings present significant steps towards furthering our understanding of elastic wave propagation and scattering within randomly heterogeneous media, and the methodology introduces a reliable basis for substantial new work in this field. The achieved numerical validation of the second order models in the wide frequency and crystallite anisotropic factor ranges has a fundamental importance due to wide applications of these models in different fields and therefore also our pursuit of achieving industrial nondestructive wave inversion techniques to infer and characterize the properties of such materials.

ACKNOWLEDGMENTS

The authors gratefully acknowledge the useful discussions with Dr. Christopher M. Kube that brought to light Ledbetter's experimental results and the support from Dr. Peter Huthwaite for his useful suggestions on modelling. Acknowledgement is also due to the free (and available for download) software packages used: for Voronoi tessellation, Neper FE, solving on the GPU, Pogo, and meshing, Gmsh. This work was partially supported by the UK Engineering and Physical Sciences Research Council (EPSRC). G.S. and S.I.R. were also partially sponsored by the AFRL (USA) under the prime Contract No. FA8650-10-D-5210.

[1]R. Hill, "The elastic behaviour of a crystalline aggregate," Proc. R. Soc. A **65**(5), 349–354 (1951).
[2]Z. Hashin and S. Shtrikman, "A variational approach to the theory of the elastic behaviour of polycrystals," J. Mech. Phys. Solids **10**(4), 343–352 (1962).
[3]W. Voigt "Theoretische studien uber die elastizitatsverhaltnisse der krystalle" ("Theoretical studies on the elastic behavior of crystals"), Abh. Kgl. Ges. Wiss. Gotingen. **34**, 3–51 (1887).
[4]R. B. Thompson, "Elastic-wave propagation in random polycrystals: Fundamentals and application to nondestructive evaluation," in *Imaging of Complex Media with Acoustic and Seismic Waves*, Topics in Applied Physics Vol. 84, edited by M. Fink, W. A. Kuperman, J.-P. Montagner, and A. Tourin (Springer-Verlag, Berlin, Germany, 2002), pp. 233–257.
[5]R. B. Thompson, F. J. Margetan, P. Haldipur, L. Yu, A. Li, P. Panetta, and H. Wasan, "Scattering of elastic waves in simple and complex polycrystals," Wave Motion **45**, 655–674 (2008).
[6]A. Van Pamel, C. R. Brett, and M. J. S. Lowe, "A methodology for evaluating detection performance of ultrasonic array imaging algorithms for coarse-grained materials," IEEE Trans. Ultrason. Ferroelect. Freq. Control. **61**, 2042–2053 (2014).
[7]M. G. Gustafsson and T. Stepinski, "Studies of split spectrum processing, optimal detection, and maximum likelihood amplitude estimation using a simple clutter model," Ultrasonics **35**, 31–52 (1997).
[8]B. Lan, M. J. S. Lowe, and F. P. E. Dunne, "Experimental and computational studies of ultrasound wave propagation in hexagonal close-packed polycrystals for texture detection," Acta Mater. **63** 107–122 (2014).
[9]Y. K. Han and R. B. Thompson, "Ultrasonic backscattering in duplex microstructures: Theory and application to titanium alloys," Metall. Mater. Trans. A **28**, 91–104 (1997).
[10]O. I. Lobkis and S. I. Rokhlin, "Characterization of polycrystals with elongated duplex microstructure by inversion of ultrasonic backscattering data," Appl. Phys. Lett. **96**(16), 161905 (2010).
[11]O. I. Lobkis, L. Yang, J. Li, and S. I. Rokhlin, "Ultrasonic backscattering in polycrystals with elongated single phase and duplex microstructure," Ultrasonics **52**(6), 694–705 (2012).
[12]L. Yang, J. Li, O. I. Lobkis, and S. I. Rokhlin, "Ultrasonic propagation and scattering in duplex microstructures with application to titanium alloys," J. Nondestruct. Eval. **31**(3), 270–283 (2012).
[13]H. Du and J. A. Turner, "Ultrasonic attenuation in pearlitic steel," Ultrasonics **54**(3), 882–887 (2014).
[14]A. L. Pilchak, J. Li, and S. I. Rokhlin, "Quantitative comparison of microtexture in near-alpha titanium measured by ultrasonic scattering and electron backscatter diffraction," Metall. Mater. Trans. A **45**(10), 4679–4697 (2014).
[15]J. A. Turner and G. Ghoshal, "Polycrystals under applied loads: Second-order grain statistics," Appl. Phys. Lett. **97**, 031907 (2010).
[16]J. Li and S. I. Rokhlin, "Elastic wave scattering in random anisotropic solids," Int. J. Solid. Struct. **78–79**, 110–124 (2016).
[17]T. Sumiya, S. Biwa, and G. Haïat, "Computational multiple scattering analysis of elastic waves in unidirectional composites," Wave Motion **50**(2), 253–270 (2013).
[18]G. Ghoshal, J. A. Turner, and R. L. Weaver, "Wigner distribution of a transducer beam pattern within a multiple scattering formalism for heterogeneous solids," J. Acoust. Soc. Am. **122**, 2009–2021 (2007).
[19]P. Hu, C. M. Kube, L. W. Koester, and J. A. Turner, "Mode-converted diffuse ultrasonic backscatter," J. Acoust. Soc. Am. **134**(2), 982–990 (2013).
[20]E. P. Papadakis, "Ultrasonic attenuation caused by scattering in polycrystalline media," in *Physical Acoustics IV: Part B*, edited by W. P. Mason (Academic Press, New York, 1968), pp. 296–328.
[21]S. Hirsekorn, "The scattering of ultrasonic waves by polycrystals," J. Acoust. Soc. Am. **72**, 1021–1031 (1982).
[22]J. B. Keller, "Stochastic equations and wave propagation in random media," in *Proceedings of Symposia in Applied Mathematics*, Vol. XVI, edited by R. Bellman (AMS, Providence, RI, 1964), pp. 145–177.
[23]F. C. Karal and J. B. Keller, "Elastic, electromagnetic, and other waves in a random medium," J. Math. Phys. **5**, 537–547 (1964).
[24]F. E. Stanke and G. S. Kino, "A unified theory for elastic wave propagation in polycrystalline materials," J. Acoust. Soc. Am. **75**, 665–681 (1984).
[25]R. L. Weaver, "Diffusivity of ultrasound in polycrystals," J. Mech. Phys. Solids **38**, 55–86 (1990).
[26]S. M. Rytov, A. Y. Kravtsov, and V. I. Tatarskii, *Principles of Statistical Radiophysics* (Springer-Verlag, New York, 1989), Vol. 4, Chap. 4, pp. 79–188.
[27]U. Frisch, "Wave propagation in random media," in *Probalistic Methods in Applied Mathematics*, edited by A. T. Barucha-Reidb (Academic Press, New York, 1968), pp. 75–198.
[28]G. Ghoshal and J. A. Turner, "Numerical model of longitudinal wave scattering in polycrystals," IEEE Trans. Ultrason. Ferroelect. Freq. Control. **56**, 1419–1428 (2009).
[29]S. Shahjahan, F. Rupin, A. Aubry, B. Chassignole, T. Fouquet, and A. Derode, "Comparison between experimental and 2-D numerical studies of multiple scattering in Inconel600 by means of array probes," Ultrasonics **54**, 358–367 (2014).
[30]A. Van Pamel, C. R. Brett, P. Huthwaite, and M. J. S. Lowe, "Finite element modelling of elastic wave scattering within a polycrystalline material in two and three dimensions," J. Acoust. Soc. Am. **138**, 2326–2336 (2015).
[31]A. Van Pamel, G. Sha, S. I. Rokhlin, and M. J. S. Lowe, "Finite element modelling of elastic wave propagation and scattering within heterogeneous media," Proc. R. Soc. A **473**, 20160738 (2016).
[32]M. Calvet and L. Margerin, "Velocity and attenuation of scalar and elastic waves in random media: A spectral function approach," J. Acoust. Soc. Am. **131**(3), 1843–1862 (2012).
[33]S. I. Rokhlin, J. Li, and G. Sha, "Far-field scattering model for wave propagation in random media," J. Acoust. Soc. Am. **137**(5), 2655–2669 (2015).
[34]C. M. Kube and J. A. Turner, "Ultrasonic attenuation in polycrystals using a self-consistent approach," Wave Motion **57**, 182–193 (2015).

[35]J. A. Turner, "Elastic waves propagation and scattering in heterogeneous, anisotropic media: Textured polycrystalline materials," J. Acoust. Soc Am. **106**, 541–552 (1999).
[36]J. Li and S. I. Rokhlin, "Propagation and scattering of ultrasonic waves in polycrystals with arbitrary crystallite and macroscopic texture symmetries," Wave Motion **58**, 145–164 (2015).
[37]R. C. Bourret, "Statistically perturbed fields, with applications to wave propagation in random media," Nuovo Cimento **26**(1), 1–31 (1962).
[38]C. S. Man, R. Paroni, Y. Xiang, and E. A. Kenik, "On the geometric autocorrelation function of polycrystalline materials," J. Comput. Appl. Math. **190**, 200–210 (2006).
[39]L. Yang, O. I. Lobkis, and S. I. Rokhlin, "Shape effect of elongated grains on ultrasonic attenuation in polycrystalline materials," Ultrasonics **51**(6), 697–708 (2011).
[40]C. M. Kube and M. de Jong, "Elastic constants of polycrystals with generally anisotropic crystals," J. Appl. Phys. **120**, 165105 (2016).
[41]P. Haldipur, F. J. Margetan, and R. B. Thompson, "Estimation of single-crystal elastic constants of polycrystalline materials from back-scattered grain noise," in *Review of Progress in Quantitative NDE*, Vol. 25, edited by D. O. Thompson and D. E. Chimenti (AIP Publishing LLC, Melville, NY, 2006), pp. 1133–1140.
[42]F. Hosford, *The Mechanics of Crystals and Textured Polycrystals* (Oxford University Press, New York, 1993), pp. 1–248.
[43]R. Quey, P. R. Dawson, and F. Barbe, "Large-scale 3D random polycrystals for the finite element method: Generation, meshing and remeshing," Comput. Methods Appl. Mech. Eng. **200**(17–20), 1729–1745 (2011).
[44]P. Huthwaite, "Accelerated finite element elastodynamic simulations using the GPU," J. Comput. Phys. **257**, 687–707 (2014).
[45]C. Geuzaine and J. F. Remacle, "Gmsh: A 3-D finite element mesh generator with built-in pre- and post-processing facilities," Int. J. Numer. Methods Eng. **79**(11), 1309–1331 (2009).
[46]H. M. Ledbetter, "Sound velocities and elastic-constant averaging for polycrystalline copper," J. Phys. D **13**, 1879–1884 (1980).